MADRID
inter.noise 2019
June 16 - 19
NOISE CONTROL FOR A BETTER ENVIRONMENT

Virtual round robin tests for uncertainty quantification of single-number ratings for the sound reduction index

Van hoorickx, Cédric[1]
Reynders, Edwin[2]

KU Leuven, Department of Civil Engineering, Structural Mechanics Section
Kasteelpark Arenberg 40 box 2448, 3001 Leuven, Belgium

ABSTRACT

As transmission loss assessment is subject to a significant variability across a range of possible facilities, virtual round robin testing is applied to assess the inherent uncertainty of a given measurement procedure on the weighted sound reduction index. The joint probability distribution of the uncertain parameters is quantified by means of a maximum entropy approach. A Monte Carlo simulation is then performed to predict the uncertainty of the sound insulation. At high frequencies, an efficient method is needed to calculate the sound transmission. A nonparametric probabilistic method is therefore developed based on the Guassian Orthogonal Ensemble (GOE), where the wall and the rooms are coupled using the spatial correlation of room modes. With the presented approach, the sound reduction index can efficiently be predicted up to high frequencies. This allows quantifying the uncertainty of the weighted sound reduction index and its spectrum adaptation terms according to ISO 717-1:2013. Application of a calcium silicate block wall shows good correspondence with indicative values for uncertainty of the weighted sound reduction index given in ISO 12999-1.

Keywords: Virtual round robin tests, uncertainty quantification, single-number rating
I-INCE Classification of Subject Number: 76

1. INTRODUCTION

Sound insulation assessment in laboratories is subject to multiple uncertain parameters, related to the measurement setup, room properties, and test sample dimensions and damping loss factors. Due to this uncertainty, differences are encountered between measurements done at different test facilities, which is referred to as reproducibility in the literature [1]. As a specific problem, the uncertainty in the direct sound reduction

[1]cedric.vanhoorickx@kuleuven.be
[2]edwin.reynders@kuleuven.be

index assessment of a building component according to ISO 10140-5 [2] is numerically studied. The measurement setup consists of a source room and a receiver room with a test element, e.g. a wall, in between. Numerous experimental round robin tests have been performed to study the variability of the performance of a wall system across several facilities, but these tests are usually expensive. In this paper, virtual round robin testing is applied. A probabilistic framework is used for quantifying the combined effect of all uncertain parameters, constructing their joint probability distribution by means of a maximum entropy approach [3]. The distribution that is obtained in this way is compatible with the available information (taken from ISO 10140-5 and literature) but otherwise maximally conservative so that no conclusions can be drawn that are not warranted by the available information.

For quantifying the uncertainty of the predicted sound transmission loss values, a Monte Carlo approach is employed. Statistically independent samples of the random parameters are generated in accordance with their joint probability distribution. For each set of generated parameter values, corresponding to a realization of a transmission suite, the sound reduction index is calculated. For predicting the sound transmission loss in a design situation, a suitable mathematical model is needed. In this paper, a novel non-parametric probabilistic method is presented based on the Gaussian Orthogonal Ensemble. The test element is modeled deterministically while the acoustic fields of the rooms are assumed diffuse. The rooms and the wall are coupled using the spatial correlation of the room modes and an analytical expression of the wall modes. The model allows computing the sound transmission in a computationally efficient way up to high frequencies, combining parametric and non-parametric uncertainty in the Monte Carlo simulation. A set of statistically independent samples of the weighted sound reduction index can then be calculated, from which its mean, variance, probability distribution, etc. can be estimated.

The paper is organized as follows. First, the prediction model is described, after which the diffuse model for the natural frequencies and modeshapes is discussed. The parametric uncertainty quantification based on the maximum entropy approach is reviewed. The paper concludes with the application of a calcium silicate block wall.

2. PREDICTION MODEL FOR AIRBORNE SOUND INSULATION

2.1. System of equations

The transmission loss is computed using the assumed-modes method, approximating the pressure fields of the source room p_1 and reveiver room p_3 and the vibration field of the wall u_2 into a finite set of basis functions:

$$p_{1/3} \approx \sum_{k=1}^{n_{1/3}} \phi_{1/3k}(x,y,z) q_{1/3k}(\omega) = \boldsymbol{\phi}_{1/3} \mathbf{q}_{1/3} \qquad u_2 \approx \sum_{k=1}^{n_2} \phi_{2k}(y,z) q_{2k}(\omega) = \boldsymbol{\phi}_2 \mathbf{q}_2 \tag{1}$$

Inserting these approximations into Lagrange's equations of motion and adopting a hysteretic damping model yields the following linear system of equations:

$$\begin{bmatrix} \mathbf{D}_{11} & \mathbf{K}_{12} & \mathbf{0} \\ \mathbf{K}_{21} & \mathbf{D}_{22} & \mathbf{K}_{23} \\ \mathbf{0} & \mathbf{K}_{32} & \mathbf{D}_{33} \end{bmatrix} \begin{Bmatrix} \mathbf{q}_1 \\ \mathbf{q}_2 \\ \mathbf{q}_3 \end{Bmatrix} = \begin{Bmatrix} \mathbf{f}_1 \\ \mathbf{0} \\ \mathbf{0} \end{Bmatrix} \tag{2}$$

where

$$\mathbf{D}_{kk} = -\omega^2 \mathbf{I}_k + \boldsymbol{\omega}_k^2 (1 + \mathrm{i}\eta_k) \tag{3}$$

with i the imaginary unit and $\boldsymbol{\omega}_k$ the diagonal matrix containing the circular undamped eigenfrequencies for subsystem k corresponding to the mode shapes in $\boldsymbol{\phi}_k$. The damping loss factors of the rooms are computed from their reverberation times via $\eta = 4.4\pi/(\omega T)$. The n_p loudspeakers are modeled as point monopoles acting at positions $(x_{\mathrm{p}j}, y_{\mathrm{p}j}, z_{\mathrm{p}j})$ with volume accelerations $a_\mathrm{p}(\omega)$. Element k of the loading vector $\mathbf{f}_1$ therefore reads

$$f_{1k}(\omega) = -\rho_\mathrm{a} a_\mathrm{p}(\omega) \sum_{j=1}^{n_\mathrm{p}} \phi_{1k}(x_{\mathrm{p}j}, y_{\mathrm{p}j}, z_{\mathrm{p}j}) \tag{4}$$

The matrices $\mathbf{K}_{12}$ and $\mathbf{K}_{32}$ are coupling matrices that represent the loading on the room due to the plate movement, and $\mathbf{K}_{21}$ and $\mathbf{K}_{23}$ represent the loading on the plate due to the room pressure. The elements of the coupling matrices are:

$$K_{21,kl} = \int_0^{L_{\mathrm{y}2}} \int_0^{L_{\mathrm{z}2}} \phi_{1l}(L_{\mathrm{x}1}, y, z)\phi_{2k}(y, z)\mathrm{d}z\mathrm{d}y \qquad K_{12,kl} = -\rho_a \omega^2 K_{21,lk} \tag{5}$$

$$K_{23,kl} = \int_0^{L_{\mathrm{y}2}} \int_0^{L_{\mathrm{z}2}} \phi_{3l}(L_{\mathrm{x}1}, y, z)\phi_{2k}(y, z)\mathrm{d}z\mathrm{d}y \qquad K_{32,kl} = -\rho_a \omega^2 K_{23,lk} \tag{6}$$

The computations require the natural frequencies and mode shapes of the subsystems to be computed. The rooms are modeled as diffuse subsystems, whose natural frequencies and mode shapes are computed in section 3. The wall is assumed to be a deterministic subsystem. Its natural frequencies are given by:

$$\omega_{2k} = \sqrt{\frac{D_2}{m_2''}} \left[\left(\frac{m_{k\mathrm{y}}\pi}{L_{\mathrm{y}2}} \right)^2 + \left(\frac{m_{k\mathrm{z}}\pi}{L_{\mathrm{z}2}} \right)^2 \right] \tag{7}$$

with D_2 the bending stiffness, m_2'' the mass of the wall per unit area, $L_{\mathrm{y}2}$ the width, and $L_{\mathrm{z}2}$ the height of the wall. The integers $m_{k\mathrm{y}}$ and $n_{k\mathrm{z}}$ represent the number of half wavelengths in the plate dimensions. The mode shapes of the wall are calculated as follows:

$$\phi_{2k} = \frac{2}{\sqrt{m_2'' L_{\mathrm{y}2} L_{\mathrm{z}2}}} \sin\left(\frac{m_{k\mathrm{y}}\pi y}{L_{\mathrm{y}2}} \right) \sin\left(\frac{m_{k\mathrm{z}}\pi z}{L_{\mathrm{z}2}} \right) = A_2 \sin\left(k_{2k\mathrm{y}} y \right) \sin\left(k_{2k\mathrm{z}} z \right) \tag{8}$$

2.2. Reducing the number of modes

In order to efficiently solve equation (2), one should note that the number of modes in the rooms is generally much higher than the number of modes in the wall between the two rooms. It is therefore advantageous to perform row reduction on the block matrices to reduce the size of the system of equations in equation (2). This yields:

$$\mathbf{A}\mathbf{q}_2 = \mathbf{b} \tag{9}$$

where the elements of the matrices $\mathbf{A}$ and $\mathbf{b}$ are given by:

$$A_{ij} = D_{22,ij} + \rho\omega^2 \sum_{k=1}^{n_1} \frac{K_{21,ik} K_{21,jk}}{D_{11,kk}} + \rho\omega^2 \sum_{k=1}^{n_3} \frac{K_{23,ik} K_{23,jk}}{D_{33,kk}} \qquad b_i = -\sum_{k=1}^{n_1} \frac{K_{21,ik} f_{1k}}{D_{11,kk}} \tag{10}$$

The energy in the source and receiver room can then be computed as:

$$E_1 = \frac{1}{\rho_\mathrm{a}} \sum_{k=1}^{n_1} \frac{\left| f_{1k} - \sum_{j=1}^{n_2} K_{12,kj} q_{2j} \right|^2}{\left| D_{11,kk} \right|^2} \qquad E_3 = \rho_\mathrm{a} \omega^4 \sum_{k=1}^{n_3} \frac{\left| \sum_{j=1}^{n_2} K_{23,jk} q_{2j} \right|^2}{\left| D_{33,kk} \right|^2} \tag{11}$$

Note that for solving the system of equations, sums are needed over expressions with $D_{11,kk}$ or $D_{33,kk}$ in the denominator. As these are very small for $\omega_{1k} \approx \omega$ and $\omega_{3k} \approx \omega$, respectively, it is sufficient to take a limited number of modes in the vicinity of the considered frequency, as the contribution of these modes dominates the summations. Under the assumption that the numerator of these sums is more or less constant in the vicinity of the considered frequencies, the relative error ϵ made by only looking at a frequency range $[\omega - a, \omega + a]$ equals:

$$\epsilon = 1 - \frac{2}{\pi} \arctan\left(\frac{2a}{\omega\eta}\right) \tag{12}$$

Only taking a limited number of modes into account leads to an underestimation of the total response. This error can be corrected for by multiplying the sums in equations (10) and (11) by a factor γ, which is given by:

$$\gamma = \frac{1}{1-\epsilon} = \frac{\pi}{2\arctan\left(\frac{2a}{\omega\eta}\right)} \tag{13}$$

2.3. Sound reduction index

The sound reduction index R is computed with the measurement formula:

$$R = 10\log_{10}\left(\frac{E_1}{V_1}\right) - 10\log_{10}\left(\frac{E_3}{V_3}\right) + 10\log_{10}\left(\frac{S_2}{A_3}\right) \tag{14}$$

in which V_1 and V_3 are the volume of the source and receiver room, S_2 is the surface area of the partition, and A_3 is the absorption of the receiver room.

Using the computed one-third octave band values of the sound reduction index in the bands with a center frequency between 100 Hz and 3150 Hz, the weighted sound reduction index R_w and the spectrum adaptation terms C, C_tr, $C_{50-3150}$, and $C_{\mathrm{tr},50-3150}$ are calculated according to ISO 717-1:2013 [4]. The uncertainty is assessed by computing the single number ratings for every realization from which the mean, standard deviation, probability density function, etc. can be calculated

3. NON-PARAMETRIC UNCERTAINTY QUANTIFICATION

The wave fields in the rooms are modeled as diffuse fields. A diffuse wave field is a random field, composed of plane waves coming from all directions, with statistically independent and uniformly distributed phases and zero-mean, uncorrelated amplitudes with equal variance [5]. High-frequency analysis methods such as statistical energy analysis (SEA) [6] rely on the wave-based or modal-based descriptions of diffuse fields. However, the conventional SEA allows only for the mean response quantities to be computed. When also the variance is of interest, an extension of the diffuse field model is necessary. Weaver [7] found that, for the generic case where the considered spatial uncertainty does not preserve symmetries, the statistics of the local eigenvalue spacings saturate to those of the Gaussian Orthogonal Ensemble (GOE) matrix from random matrix theory [8]. The GOE model can be used to obtain the mean and variance of a subsystem's total energy.

3.1. Natural frequencies of a diffuse acoustic volume

The following analysis is concerned with the response of a finite acoustic volume in a frequency range for which the GOE model is valid. As in this frequency range, the statistics of the local eigenvalue spacings saturate to those of the GOE, a nonparametric description of the spacings distribution can be used. The frequency range of interest is assumed finite, with a lower bound ω_l and an upper boud ω_u. For a specific subsystem, the expected total number N_int of eigenvalues in the frequency range of interest can be determined as:

$$N_\mathrm{int} = \int_{\lambda_\mathrm{l}}^{\lambda_\mathrm{u}} n^\lambda(\lambda)\mathrm{d}\lambda = \int_{\omega_\mathrm{l}}^{\omega_\mathrm{u}} n(\omega)\mathrm{d}\omega, \tag{15}$$

where $\lambda := \omega^2$, and $n^\lambda(\lambda)$ represents the local eigenvalue density, which is related to the modal density by

$$n^\lambda(\omega^2) = \frac{n(\omega)}{2\omega}. \tag{16}$$

The GOE matrix $\mathbf{G}_{n_\mathrm{G}}(\sigma_\mathrm{G})$ is a real symmetric matrix with dimensions $n_\mathrm{G} \times n_\mathrm{G}$. The elements with different indices are independent, centered Gaussian random variables. The diagonal elements have variance $2\sigma_\mathrm{G}^2$ and the off-diagonal elements have variance σ_G^2, where the parameter σ_G serves to specify an eigenvalue scale. Because $\mathbf{G}_{n_\mathrm{G}}(\sigma_\mathrm{G})$ is real and symmetric, it has n_G eigenvalues $\lambda_{\mathrm{G}r}$ that are purely real.

Wigner has shown [9] that the density of the eigenvalues λ_G of the GOE matrix $n_\mathrm{G}^\lambda(\lambda_\mathrm{G})$, which are real and centered around zero, converges, for $n_\mathrm{G} \to \infty$, to

$$n_\mathrm{G}^\lambda(\lambda_\mathrm{G}) = \frac{2n_\mathrm{G}}{\pi r}\sqrt{1 - \frac{\lambda_\mathrm{G}^2}{r^2}}, \qquad -r < \lambda_\mathrm{G} < r, \tag{17}$$

with $r := 2\sigma_\mathrm{G}\sqrt{n_\mathrm{G}}$. The cumulative count function of GOE eigenvalues in the range $[-\lambda_\mathrm{Gu}, \lambda_\mathrm{G}]$ therefore equals

$$N_\mathrm{G}(\lambda_\mathrm{G}) = \frac{n_\mathrm{G}}{\pi r^2}\left(\lambda_\mathrm{Gu}\sqrt{r^2 - \lambda_\mathrm{Gu}^2} + \lambda_\mathrm{G}\sqrt{r^2 - \lambda_\mathrm{G}^2} + r^2\left(\arctan\frac{\lambda_\mathrm{Gu}}{\sqrt{r^2 - \lambda_\mathrm{Gu}^2}} + \arctan\frac{\lambda_\mathrm{G}}{\sqrt{r^2 - \lambda_\mathrm{G}^2}}\right)\right) \tag{18}$$

To obtain a monotonically increasing function $N_\mathrm{G}(\lambda_\mathrm{G})$ in the range $[0, N_\mathrm{int}]$, λ_Gu is numerically computed by imposing $N_\mathrm{G}(\lambda_\mathrm{Gu}) = N_\mathrm{int}$.

The cumulative count function of acoustic eigenvalues in the range of interest $[\lambda_\mathrm{l}, \lambda_\mathrm{u}]$ is obtained as

$$N(\lambda) = \int_{\lambda_\mathrm{l}}^{\lambda} n^\lambda(\lambda)\mathrm{d}\lambda. \tag{19}$$

This is a monotonically increasing function (just as $N_\mathrm{G}(\lambda_\mathrm{G})$) and therefore invertible. The range is again $[0, N_\mathrm{int}]$. Application of the inverse function to the uniform random variables then yields a set of eigenvalues λ for the physical system having the correct density $n^\lambda(\lambda)$:

$$\lambda = N^{-1}\left(N_\mathrm{G}(\lambda_\mathrm{G})\right). \tag{20}$$

In summary, a set of eigenvalue realizations for the acoustic volume is obtained as follows. The number of expected eigenvalues in the frequency range of interest N_int is first computed from (15). Then, for a realization of the GOE matrix, its eigenvalues are

computed and the range $[-\lambda_{\mathrm{Gu}}, \lambda_{\mathrm{Gu}}]$ is obtained from imposing $N_{\mathrm{G}}(\lambda_{\mathrm{Gu}}) = N_{\mathrm{int}}$. Finally, the GOE eigenvalue realizations are transformed into acoustic eigenvalue realizations using (20). This procedure can be performed for the entire frequency range of interest $[\lambda_{\mathrm{l}}, \lambda_{\mathrm{u}}]$ or for different frequency intervals in order to decrease the size of the GOE matrices and therefore the computation cost of their eigenvalues. An important advantage of the this procedure is that the normalized GOE eigenvalue spacings do not depend on any physical property. This implies that the computed realizations can be tabulated and re-used.

3.2. Mode shapes of a diffuse acoustic volume

The mode shapes of a room in high-frequency regime can be interpreted as standing waves that arise from many traveling plane wave components. Adopting a diffuse acoustic field model, the pressure mode shape at a given location consists of a summation of independent plane acoustic waves with the same mean amplitude and uncorrelated phases, coming from all directions with equal probability. It then follows from the central limit theorem that the acoustic mode shapes are zero-mean, Gaussian random fields. A zero-mean Gaussian random field is uniquely determined by its covariance function.

For diffuse reflecting boundaries, the mode shapes φ_{sr} are statistically homogenous, i.e., the statistics of the pressure mode shape components are independent of their position. The corresponding random wave field is a diffuse field. For three-dimensional volumes, its covariance function then has the form [10]:

$$\mathbf{C}_{sr}\left(\mathbf{x}, \mathbf{x}'\right) = \begin{cases} A_s \mathrm{j}_0\left(k_{sr}|\mathbf{x} - \mathbf{x}'|\right) & \text{for 2 points in the acoustic room} \\ 2A_s \mathrm{j}_0\left(k_{sr}|\mathbf{x} - \mathbf{x}'|\right) & \text{for 2 points on a reflecting boundary} \end{cases} \tag{21}$$

where $\mathrm{j}_0(x) = \sin(x)/x$ is the spherical Bessel function of the first kind and order zero, $k_{sr} := \frac{2\pi}{\lambda_{sr}}$ denotes the wavenumber corresponding to the wavelength λ_{sr} of mode r for subsystem s, and A_s is a factor that is independent of position, which can be determined from the mode shape normalization condition. In an acoustic enclosure Ω with volume V_s, the normalization condition reads:

$$\int_{\Omega} \frac{1}{c^2} {\varphi_{sr}}^2(\mathbf{x}) \mathrm{d}\mathbf{x} = 1 \qquad \Leftrightarrow \qquad A_s = \frac{c^2}{V_s}. \tag{22}$$

The correlation function (21) depends only on the distance between the considered mode shape components, the wavelength and the total volume. Close to perfect reflecting boundaries, the mean squared sound pressure is twice the mean squared sound pressure in the center of the room [11]. Because of this, a factor two appears in the covariance function (21) for points located on the reflecting structural element [12].

Realizations of the mode shape vector $\varphi_{sr}(\mathbf{x})$ can be obtained from a discrete Karhunen-Loève decomposition: with the eigenvalue decomposition of the covariance matrix

$$\mathbf{C}_{sr} := \mathbf{A}\mathbf{\Sigma}\mathbf{A}^T. \tag{23}$$

the corresponding mode shape vector is

$$\varphi_{sr} := \mathbf{A}\mathbf{\Sigma}^{\frac{1}{2}}\boldsymbol{\xi}, \tag{24}$$

where $\boldsymbol{\xi}$ is a vector of independent, standard normal random variables that can be realized with a Gaussian random number generator.

However, to compute the coupling matrices in equations (5) and (6), the mode shapes are needed over the wall surface, which requires a fine mesh, especially at high frequencies. This implies a large covariance matrix and therefore a computationally expensive eigenvalue decomposition. To reduce the computational cost, the wave field close to the wall is assumed to be statistically uncorrelated from the wave field at the loudspeaker positions, which is reasonable as the loudspeakers are located at a significant distance from the wall and the covariance matrix in equation (21) decreases strongly with distance. Therefore, the discrete Karhunen-Loève decomposition is used to obtain the mode shapes at the positions of the loudspeakers in order to compute the loading vector in equation (4). The coupling matrices are computed independently as outlined in the next subsection.

3.3. Computation of the coupling matrices

Instead of numerically evaluating the integrals in equations (5) and (6), the statistics of the coupling matrices are computed directly. When integrating a Gaussian field, it is the limit of a linear combination of Gaussian random variables so it is again Gaussian. The entries of the coupling matrix are therefore Gaussian variables and are determined by their mean and variance. As the mean of the mode shapes equals zero, also the mean of the coupling matrices equals zero. The variance of $K_{21,kl}$ is computed as follows:

$$\mathrm{Var}\left(K_{21,kl}\right) = \iiiint \mathrm{E}\left[\phi_{1l}(L_{\mathrm{x}1}, y, z)\phi_{1l}(L_{\mathrm{x}1}, y', z')\right]\phi_{2k}(y, z)\phi_{2k}(y', z')\mathrm{d}z'\mathrm{d}z\mathrm{d}y'\mathrm{d}y \tag{25}$$

as the mode shapes of the wall (subsystem 2) are deterministic. As the term $\mathrm{E}\left[\phi_{1l}(L_{\mathrm{x}1}, y, z)\phi_{1l}(L_{\mathrm{x}1}, y', z')\right]$ is the covariance function for two points on a reflecting boundary (equation (21)), this integral becomes:

$$\begin{aligned}&\mathrm{Var}\left(K_{21,kl}\right)\\ &= 2A_1A_2^2 \iiiint \mathrm{j}_0\left(k_{1l}|\mathbf{x}-\mathbf{x}'|\right)\sin\left(k_{2k\mathrm{y}}y\right)\sin\left(k_{2k\mathrm{y}}y'\right)\sin\left(k_{2k\mathrm{z}}z\right)\sin\left(k_{2k\mathrm{z}}z'\right)\mathrm{d}z'\mathrm{d}z\mathrm{d}y'\mathrm{d}y\end{aligned} \tag{26}$$

where the integrals go from 0 to $L_{\mathrm{y}2}$ for the ones in y and y' and from 0 to $L_{\mathrm{z}2}$ for the ones in z and z'. The distance function in the spherical Bessel function is given by $|\mathbf{x}-\mathbf{x}'| = \sqrt{(y-y')^2+(z-z')^2}$. The quadruple integral equals the following double integral:

$$\mathrm{Var}\left(K_{21,kl}\right) = 2A_1A_2^2L_{\mathrm{y}2}^2L_{\mathrm{z}2}^2 \int_0^1\int_0^1 \mathrm{j}_0\left(a_{1l\mathrm{y}}\sqrt{u^2+\gamma^2v^2}\right)h\left(a_{2k\mathrm{y}}, u\right)h\left(a_{2k\mathrm{z}}, v\right)\mathrm{d}v\mathrm{d}u \tag{27}$$

with $a_{1l\mathrm{y}} = k_{1l}L_{\mathrm{y}2}$, $\gamma = L_{\mathrm{z}2}/L_{\mathrm{y}2}$, $a_{2k\mathrm{y}} = k_{2k\mathrm{y}}L_{\mathrm{y}2}$, $a_{2k\mathrm{y}} = k_{2k\mathrm{z}}L_{\mathrm{z}2}$, and:

$$h\left(a, u\right) = (1-u)\cos\left(au\right) - \frac{\cos\left(a\right)}{a}\sin\left(a(1-u)\right) \tag{28}$$

The integral in equation (27) is evaluated numerically at every realization. To reduce the computational cost, this integral is only evaluated for a limited number of $a_{1l\mathrm{y}}$ (e.g. 200 linearly spaced values) as the value of the variance $\mathrm{Var}\left(K_{21,kl}\right)$ changes smoothly over the frequency. Linear interpolation then yields the variance for intermediate values of $a_{1l\mathrm{y}}$.

4. PARAMETRIC UNCERTAINTY QUANTIFICATION

The maximum entropy principle is a powerful tool that enables constructing the most conservative probability density function of a parameter that is compatible with all available imprecise information, such as bounds and expected values. Most of the uncertain variables in a sound insulation prediction problem can be represented by continuous random variables. The information measure of the probability distribution function $p(x)$ of a continuous random variable x that takes values in $\mathcal{D} \subseteq \mathbb{R}$, can be defined as:

$$H\left(p(x)\right) := -\int_{\mathcal{D}} p(x) \log\left(\frac{p(x)}{m(x)}\right) \mathrm{d}x, \tag{29}$$

with $m(x)$ Jaynes' *invariant measure* function, taken to be a uniform distribution over the interval $\mathcal{D}$. The probability distribution function is furthermore subject to one or more of the following constraints:

$$\int_{\mathcal{D}} x^m p(x) \mathrm{d}x = \mu\left(x^m\right), \quad m = 0, 1, 2, \tag{30}$$

The probability distribution that is compatible with the available information but otherwise minimally informative (or maximally uncertain) is obtained by maximizing the entropy function in equation (29) under the constraints provided by the information [13]. Note that when the available information relates multiple random variables of the sound insulation prediction problem, they are statistically dependent so that their joint distribution will in general be different from the product of their marginal distributions.

The maximum entropy framework is employed for constructing probability distributions of the physical parameters that govern the airborne sound insulation of building elements tested in laboratory conditions. The rooms of the uncertain test facility are assumed to comply with ISO 10140-5 [2]. The uncertain parameters of the rooms are the volume, the dimensions and the reverberation time. For the test element, the probability distributions of the dimensions and the total loss factor are obtained using the maximum entropy framework. Also the probability distributions for the measurement setup, i.e. the number of loudspeakers and their position, are obtained in this way. Details on the obtained probability distributions for the room properties, the test element properties, and the measurement setup can be found in [13].

5. APPLICATION

A heavy single-leaf wall, for which experimental results obtained in multiple laboratories have been reported in the literature, is studied. The wall has a thickness of 25 cm and consists of calcium silicate blocks with mass density $\rho = 1800\,\mathrm{kg/m^3}$, Young's modulus $E = 10.8\,\mathrm{GPa}$, and Poisson's ratio $\nu = 0.2$. As assuming a diffuse field overestimates the variance at low frequencies [14], a deterministic model based on the hard-walled modes is used for the rooms for frequencies up to 225 Hz. The mean of the predicted sound transmission loss and the corresponding 95 % confidence interval for 2000 Monte Carlo simulations are shown in figure 1.

At low frequencies, the modal density of the wall, measured across the random ensemble, is generally low. The first natural frequency of the wall is a random variable that takes values between 56.5 Hz and 70 Hz. Its probability distribution shows a sharp peak at 57 Hz, resulting in a pronounced dip in the statistics of the sound transmission

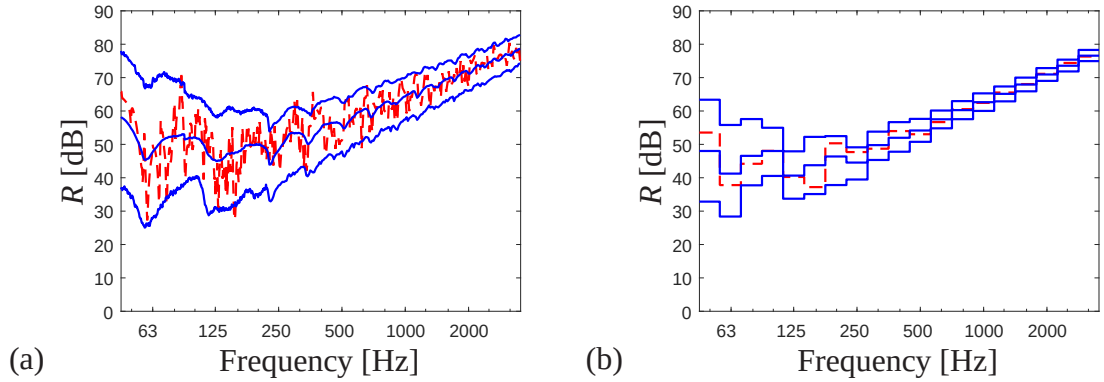

Figure 1: Predicted sound transmission loss for a calcium silicate block wall: (a) harmonic and (b) one-third octave band results. Solid blue line: mean and 95 % *confidence interval, obtained from 2000 Monte Carlo realizations. Dashed red line: result for a single realization.*

loss at the same frequency. At higher frequencies, the modal density increases and the dips caused by individual wall modes become less pronounced. The critical frequency of the wall is at 102.5 Hz, yet no clear coincidence dip is observed because the modal density is low and varies strongly with frequency. Behind the critical frequency, the transmission loss increases between 7 dB and 9 dB per octave.

The uncertainty of the harmonic transmission loss predictions is very large, especially at low frequencies. Band averaging reduces the uncertainty, but as can be observed in figure 1b, the uncertainty remains important. The 95 % confidence intervals of both walls are plotted in figure 2 together with the measured values from Meier [15] and indicative values from ISO 140-2 [1], ISO 12999-1 [16], and Hongisto et al. [17]. These indicative values are based on a limited number of inter-laboratory experiments for different wall types, and provide a rough indication of the accuracy that can be expected. The large difference in the 160 Hz and 200 Hz bands indicates a larger uncertainty than would be expected from the indicative values. This is a result of the large difference in performance for these one-third octave bands when no wall modes or one or two modes are present.

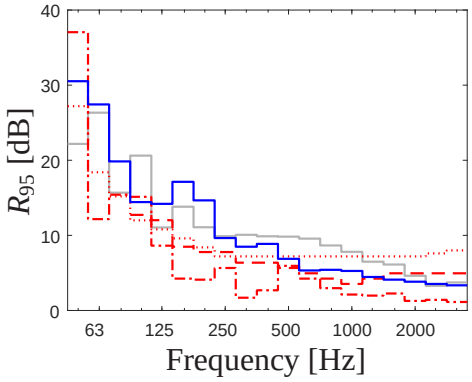

Figure 2: 95 % *confidence interval of the predicted sound transmission loss for the calcium silicate wall (solid blue line). These are compared with the values corresponding to the* 95 % *confidence interval of the measured sound transmission loss [15] (solid gray line) and with the values corresponding to the reproducibility of inter-laboratory tests as listed in ISO 140-2 [1] (dashed red line), ISO 12999-1 [16] (dotted red line) and Hongisto et al. [17] (dash-dotted red line).*

Figure 3 displays the probability distribution of the single number ratings. This

figure shows that $\mathrm{E}[R_\mathrm{w}] > \mathrm{E}[R_\mathrm{w}+C] > \mathrm{E}[R_\mathrm{w}+C_\mathrm{tr}]$, as can be expected, and $\mathrm{Var}(R_\mathrm{w}) < \mathrm{Var}(R_\mathrm{w}+C) < \mathrm{Var}(R_\mathrm{w}+C_\mathrm{tr})$, which is in correspondence with the findings of Wittstock [18]. Table 1 lists the mean and 95 % confidence interval for the different single number ratings. The 95 % confidence interval is in line with the indicative values from ISO 12999-1 [16]: 2.0 dB for R_w, 2.1 dB for $R_\mathrm{w}+C$ and $R_\mathrm{w}+C_{50-3150}$, and 2.4 dB for $R_\mathrm{w}+C_\mathrm{tr}$ and $R_\mathrm{w}+C_{\mathrm{tr},50-3150}$.

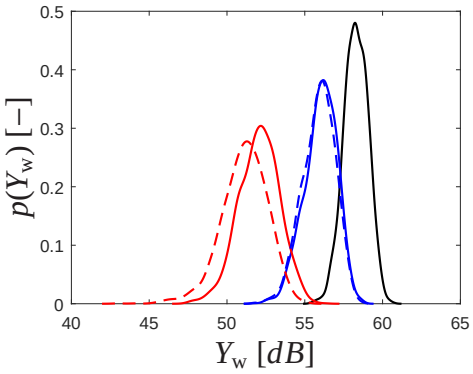

Figure 3: Probability distribution of the single number ratings Y_w: R_w (solid black line), $R_\mathrm{w}+C$ (solid blue line), $R_\mathrm{w}+C_\mathrm{tr}$ (solid red line), $R_\mathrm{w}+C_{50-3150}$ (dashed blue line), $R_\mathrm{w}+C_{\mathrm{tr},50-3150}$ (dashed red line).

Table 1: Mean and 95 % confidence interval of the single number ratings for the calcium silicate block wall.

R_w [dB]	$R_\mathrm{w}+C$ [dB]	$R_\mathrm{w}+C_\mathrm{tr}$ [dB]	$R_\mathrm{w}+C_{50-3150}$ [dB]	$R_\mathrm{w}+C_{\mathrm{tr},50-3150}$ [dB]
58.3 ± 1.5	56.0 ± 1.9	52.1 ± 2.6	55.9 ± 2.0	51.1 ± 2.9

6. CONCLUSIONS

In this paper, a probabilistic framework is presented for quantifying the variability of the sound insulation assessment across a range of possible test facilities that satisfy the ISO 10140-5 standard. The framework combines parametric uncertainty quantified using the maximum entropy principle and nonparametric uncertainty resulting from the assumption of diffuse fields in the rooms. The diffuse wave model is based on the Gaussian Orthogonal Ensemble and on the assumption of Gaussian distributed acoustic mode shapes. The approach is applied to the prediction of the airborne sound insulation of a calcium silicate block wall. The method allows computing the probability distribution of the sound transmission loss for the acoustic frequency range. As a result, the mean and the uncertainty of single number ratings can be computed.

7. ACKNOWLEDGEMENTS

The research presented in this paper has been performed within the frame of the VirBAcous project (project ID 714591) “Virtual building acoustics: a robust and efficient analysis and optimization framework for noise transmission reduction” funded by the European Research Council in the form of an ERC Starting Grant. The financial support is gratefully acknowledged.

8. REFERENCES

[1] International Organization for Standardization. *ISO 140-2:1991: Acoustics – Measurement of sound insulation in buildings and of building elements – Part 2: Determination, verification and application of precision data*, 1991.

[2] International Organization for Standardization. *ISO 10140-5:2010: Acoustics – Laboratory measurement of sound insulation of building elements – Part 5: Requirements for test facilities and equipment*, 2010.

[3] E.T. Jaynes. *Probability Theory. The Logic of Science*. Cambridge University Press, Cambridge, UK, 2003.

[4] International Organization for Standardization. *ISO 717-1:2013: Acoustics – Rating of sound insulation in buildings and of building elements – Part 1: Airborne sound insulation*, 2013.

[5] K.J. Ebeling. Statistical properties of random wave fields. In W.P. Mason and R.N. Thurston, editors, *Physical acoustics Vol. XVII*, pages 233–310. Academic Press, Orlando, FL, 1984.

[6] R.H. Lyon and R.G. DeJong. *Theory and application of statistical energy analysis*. Butterworth-Heinemann, Newton, MA, second edition, 1995.

[7] R.L. Weaver. On the ensemble variance of reverberation room transmission functions, the effect of spectral rigidity. *Journal of Sound and Vibration*, 130(3):487–491, 1989.

[8] M.L. Mehta. *Random Matrices*. Elsevier, San Diego, CA, 3rd edition, 2004.

[9] E.P. Wigner. On the distribution of the roots of certain symmetric matrices. *Annals of Mathematics*, 67(2):325–327, 1958.

[10] R.K. Cook, R.V. Waterhouse, R.D. Berendt, S. Edelman, and M.C. Thompson Jr. Measurement of correlation coefficients in reverberant sound fields. *Journal of the Acoustical Society of America*, 27(6):1072–1077, 1955.

[11] R.V. Waterhouse. Interference patterns in reverberant sound fields. *Journal of the Acoustical Society of America*, 27(2):247–258, 1955.

[12] J.H. Rindel. *Sound insulation in buildings*. CRC Press, Boca Raton, FL, 2018.

[13] E. Reynders. Parametric uncertainty quantification of sound insulation values. *Journal of the Acoustical Society of America*, 135(4):1907–1918, 2014.

[14] C. Van hoorickx and E. Reynders. Uncertainty quantification of sound transmission measurement procedures based on the Gaussian Orthogonal Ensemble. In D. Herrin, J. Cuschieri, and G. Ebbitt, editors, *Proceedings of the 47th International Congress and Exposition on Noise Control Engineering, Inter-Noise 2018*, Chicago, USA, August 2018. CD-ROM.

[15] A. Meier, A. Schmitz, and G. Raabe. Inter-laboratory test of sound insulation measurements on heavy walls: Part II - results of main test. *Building Acoustics*, 6(3–4):171–186, 1999.

[16] International Organization for Standardization. *ISO 12999-1:2014: Acoustics – Determination and application of measurement uncertainties in building acoustics – Part 1: Sound insulation*, 2014.

[17] V. Hongisto, J. Keränen, M. Kylliäinen, and J. Mahn. Reproducibility of the present and the proposed single-number quantities of airborne sound insulation. *Acta Acustica united with Acustica*, 98(5):811–819, 2012.

[18] V. Wittstock. On the uncertainty of single-number quantities for rating airborne sound insulation. *Applied Acoustics*, 93(3):375–386, 2007.